X-ray photoemission spectroscopy characterization of the electrode-ferroelectric interfaces in Pt/$Bi_4Ti_3O_{12}$/Pt and Pt/$Bi_{3.25}La_{0.75}Ti_3O_{12}$/Pt capacitors: Possible influence of defect structure on fatigue properties

M.-W. Chu,* M. Ganne, M. T. Caldes,† E. Gautier, and L. Brohan
Institut des Matériaux Jean Rouxel UMR 6502, Laboratoire de Chimie des Solides,
2 rue de la Houssinière B. P. 32229, 44322 Nantes Cedex 3, France
(Received 5 July 2002; published 8 July 2003)

The interaction between Pt electrodes and ferroelectrics in Pt/$Bi_4Ti_3O_{12}$(BTO)/Pt and Pt/$Bi_{3.25}La_{0.75}Ti_3O_{12}$(BLT)/Pt capacitors was investigated by *ex situ* x-ray photoelectron spectroscopy studies. The bare surface of crystals in BTO thin films consists of the regular Aurivillius structure, whereas that in BLT is composed of the intergrowth defects. At the annealed Pt-BTO and Pt-BLT interfaces,the Pt substitution at the BTO and BLT lattices results in Pt impurity defects, which can combine with oxygen vacancies ($V_O^{\cdot\cdot}$) resulting in complex metal-impurity-oxygen-vacancy defect pairs. The complex defect pairs at the Pt-BTO interfaces are polar, nonswitchable, and able to pin polarizations of surrounding lattices inducing fatigue. In contrast, the intergrowth defects of BLT crystals behave as an intrinsic diffusion barrier to Pt, and therefore, the harmful defect pairs occurring at the Pt-BTO interfaces are practically absent for the Pt-BLT interfaces, which could be relevant to the reported different fatigue properties of BTO and BLT capacitors.

DOI: 10.1103/PhysRevB.68.014102 PACS number(s): 61.72.Ji, 61.72.Hh, 68.35.Dv, 68.35.Fx

I. INTRODUCTION

The ferroelectric random access memory has attracted much attention during the last few decades due to its lower power requirements, faster access speed, and nonvolatility.[1,2] Early studies were primarily dedicated to the Pb(Zr_xTi_{1-x})O_3 (PZT) solid solution because of their large remanent polarization, low processing temperature, and compatibility with silicon technology.[1,2] However, PZT suffers fatigue failure, namely the decrease in switchable polarization, on metal electrodes (usually Pt) after bipolar reversals.[1,2] Although the fatigue properties of PZT can be significantly improved via the use of conductive-oxide electrodes, e.g., RuO_2 (Ref. 3) and La-Sr-Co-O,[4,5] the leakage current of such devices is relatively high (detailed reviews have been reported by several authors, e.g., Tagantsev *et al.*[6]).

The ferroelectric Aurivillius phases $SrBi_2Ta_2O_9$ (SBT, $n=2$) (Ref. 1) and $Bi_{3.25}La_{0.75}Ti_3O_{12}$ (BLT, $n=3$),[2] which consist of "n" layers of perovskite-like blocks sandwiched between two consecutive fluorite-like $(Bi_2O_2)^{2+}$ layers, have been recently explored as substituting materials for PZT, because they show good fatigue resistance and low leakage current on Pt electrode(s). In particular, BLT is regarded as a promising candidate due to its high remanent polarization.[2,7] Figure 1 shows the monoclinic crystal structure of $Bi_4Ti_3O_{12}$ (BTO, space group $B1a1$, No. 7),[8] which is the parent phase of monoclinic BLT.[9,10]

Although the origin of fatigue in Pt/PZT/Pt capacitors remains controversial,[6,11] two different mechanisms were claimed to be responsible for this phenomenon: (i) domain wall pinning within ferroelectrics by oxygen vacancies ($V_O^{\cdot\cdot}$) and (ii) electron injection near interfaces.[6] However, a number of experiments (reviewed in Ref. 6) indicated that fatigue properties did not show monotonical dependence on the concentration increase of $V_O^{\cdot\cdot}$. Instead, the existence of a low-dielectric constant or nonswitching layer in the nearby Pt-PZT interfacial region appears to be associated with fatigue.[3–6,12–16] This interfacial layer behaves as an effective electron injection site, and the injected electrons are trapped by ferroelectrics, leading to defects. Such defects then participate in the suppression of switchable polarization that results in the fatigue of PZT.[6,12,13] This electron-injection model, i.e., mechanism (ii), is also referred to as "the interface scenario".[6,12–14] Nevertheless, the detailed defect chem-

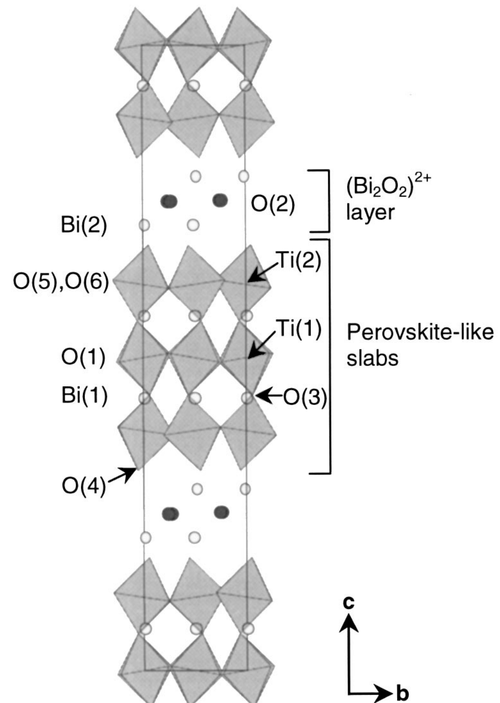

FIG. 1. The monoclinic crystal structure of $Bi_4Ti_3O_{12}$ (BTO), viewed along [100] (Ref. 8).

 ©2003 The American Physical Society

istry of this interface scenario was first reported in Pöykkö *et al.*'s first-principles total energy study,[15] which indicated that defects at the Pt-ferroelectrics interface(s) consist of dipolar metal-impurity-oxygen-vacancy pairs ($Pt_{Ti}'' - V_O^{\cdot\cdot}$), and $Pt_{Ti}'' - V_O^{\cdot\cdot}$ pairs arise from the electron trapping on virgin doubly-charged $Pt_{Ti}'' - V_O^{\cdot\cdot}$ centers.

Concerning the fatigue resistance of Aurivillius-based ferroelectric capacitors using Pt electrode(s), four possible mechanisms have been reported: (a) the oxygen stability of perovskite-like slabs being favored by Bi-free environment,[17] (b) domain wall unpinning happening at least as rapid as domain wall pinning,[18–21] (c) the self-regulating $(Bi_2O_2)^{2+}$ layer compensating for space charges near the Pt electrode(s),[1] and (d) surface configurations of crystals inducing specific Pt-ferroelectrics interface properties.[22,23] The first and second mechanisms are inferred from the domain wall pinning (by $V_O^{\cdot\cdot}$) model of Pt/PZT/Pt capacitors,[17–21] and $V_O^{\cdot\cdot}$ in Aurivillius phases are indicated to result from the fragility of Bi-O bonds and the volatilization of bismuth.[17] Park *et al.*[17] thus claimed that the absence of bismuth in the perovskite-like slabs of Aurivillius phases, e.g., SBT, is crucial for obtaining fatigue-free properties, which is referred to as mechanism (a). However, this mechanism fails for fatigue-resistant BLT, which contains a significant amount of bismuth in its perovskite-like slabs, $(Bi_{1.25}La_{0.75}Ti_3O_{10})^{2-}$. Taking the failure of mechanism (a) into account, we can suggest that domain wall pinning may not play the predominant role in fatigue properties of the Aurivillius compounds. Consequently, a further examination of the correlation between the dielectric constants and fatigue properties of SBT and BLT would be essential to confirm mechanism (b), because domain wall pinning within ferroelectrics would raise domain density, leading to an increase in the dielectric constant.[6,13,14] Furthermore, mechanism (c) should not be taken into further consideration, since Pt/BTO/Pt capacitors exhibit fatigue degradation.[24,25] In contrast to mechanisms (a)–(c) derived from macroscopic electrical[1,18–21] and spectroscopic[17] studies, the atomic-scale characterization of defect structures on the crystal surfaces of SBT (Ref. [22]) and BLT (Refs. 10 and 23) gives rise to mechanism (d). The surface structure of SBT was reported to consist of an incomplete $(Bi_2O_2)^{2+}$ layer with a top surface of oxygen atoms,[22] and that of BLT is composed of an ordered stacking of $(Bi,La)BiO_3$ and $(Bi,La)TiO_3$ deficient perovskites [see Fig. 2, and compare Fig. 2(a) with Fig. 2(b)].[10] Note that the defect structure of BLT appears within a thickness of ~5 nm from the crystal surface to bulk, whereas the BTO (fatigue)[24,25] surface always exhibits the regular Aurivillius structure.[10] The surface defects of SBT and BLT locally change the chemical composition of crystal surfaces, and the physical characteristics of the SBT and BLT crystal surfaces are thus different from those of the bulks with the regular Aurivillius structure. Consequently, the Pt-SBT and Pt-BLT interfaces should possess different properties compared to those of Pt-BTO. This feature could be associated with the distinct fatigue behaviors of SBT,[18–20] BLT,[2,21] and BTO (Refs. 24 and 25) capacitors. Therefore, mechanism (*d*) is relevant to "the interface scenario" of Pt/PZT/Pt capacitors,[6,12–14] and Pt-SBT, Pt-BLT, and Pt-BTO interface

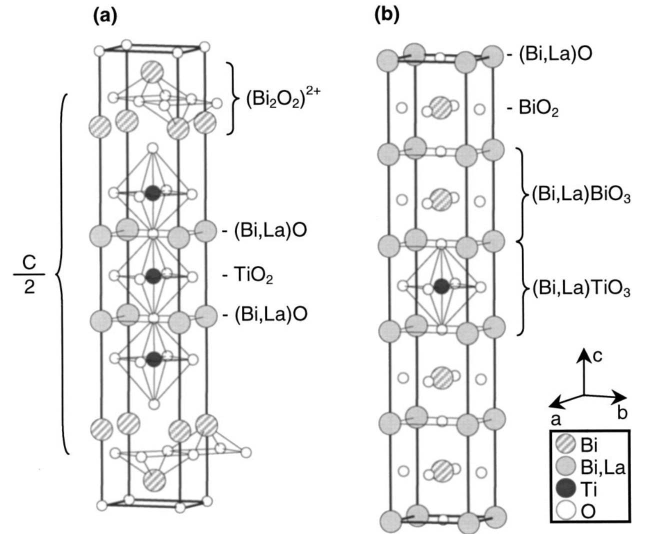

FIG. 2. Schematic structural models for (a) the regular and (b) the surface intergrowth defects of $Bi_{3.25}La_{0.75}Ti_3O_{12}$ (BLT) (Ref. 10). For simplicity, all perovskite blocks are drawn in cubic symmetry and cation vacancies (V_{Bi}''' and/or V_{La}''') in (Bi,La)O and BiO_2 planes of the intergrowth defects are not indicated.

studies are indispensable to give a further insight into the defect chemistry of this mechanism.

This paper concentrates on BTO and BLT, i.e., the Aurivillius phases with $n=3$, and reports concrete evidence for distinct defect structures at the Pt-BTO and Pt-BLT interfaces via *ex situ* X-ray photoelectron spectroscopy (XPS) studies (described in more details in Sec. II), and the Pt-SBT interface study is already in progress.

II. EXPERIMENT

Ferroelectric BTO and BLT films with a thickness of ~300 nm were prepared via chemical solution deposition on $Pt(111)/TiO_2/SiO_2/Si(100)$ substrates, which were then crystallized at 650 °C for 10 min in flowing O_2, leading to polycrystalline and stoichiometric films.[26]

For Aurivillius phases, the ion sputtering can result in reduced bismuth species[17,23] then inducing undesirable modifications to the physical and chemical natures of the Pt-BTO and Pt-BLT interfaces, and the conventional depth-profile interface study is thus not suitable. Consequently, we simulated top-and bottom-electrode interfaces in Pt/BTO/Pt and Pt/BLT/Pt capacitors by sputtering thin Pt overlayers of ~5, 10, and 20 Å on the surfaces of bare BTO and BLT films. The as-prepared samples were thermally equilibrated for $\frac{1}{2}$ h in the sputtering apparatus, and then immediately inserted into the XPS apparatus for "virgin" interface studies, qualitatively equivalent to top-electrode interfaces. To further analyze the effects of post-annealing on top-electrode interfaces (generally performed after deposition of the top electrodes), the as-analyzed "virgin" samples were heated at 400 °C for 5 min in flowing O_2 in a preheated tubular furnace, then immediately studied by XPS. These analyzed samples then underwent a second heat treatment at 650 °C for 10 min in flowing O_2 in order to create the equivalent bottom-electrode

TABLE I. XPS quantification results of bare BTO and BLT films.

Samples	Bi (at. %)	La (at. %)	Ti (at. %)	O (at. %)
BTO nominal	21.1	-	15.8	63.1
BTO powders[a]	33.1	-	4.1	62.8
BTO	33.1	-	7.5	59.4
BLT nominal	17.1	4.0	15.8	63.1
BLT powders[a]	28.0	5.5	3.9	62.6
BLT	24.9	8.0	7.8	59.3

[a]Data from powder compounds in Ref. 23.

interfaces for further XPS studies. Since the deposition and heat treatments of the thin Pt overlayers were not carried out in the XPS apparatus, we refer to this as an *ex situ* XPS study. In each case, the three steps—"virgin", 400 °C-annealed, and 650 °C-annealed Pt-BTO and Pt-BLT interface studies—were performed on the same sample, which ensures the fixed initial Pt thickness. These "*ex-situ*" XPS studies were repeated several times, and the good reproducibility of core-level spectra suggests that these simulated interfaces are *a priori* representative of the actual ones.

XPS measurements were recorded on an ESCA LEYBOLD LH12 apparatus (Université de Nantes-CNRS) using Mg $K\alpha$ radiation (1253.6 eV), and the nominal energy resolution was set to 0.89 eV, allowing the escape depth (λ) of ~15 Å for Pt $4f$ photoelectrons.[27] The operating vacuum pressure was always maintained at less than 10^{-9} Torr. The C $1s$ (284.6 eV) peak[28] of the surface carbon contamination was taken as the internal reference for spectral calibration, as the charging effects of dielectric materials are difficult to overcome.[23,29] All core levels were subjected to satellite subtraction and linear background removal before spectrum deconvolution. In addition, no surface cleaning by Ar^+ sputtering was performed.

III. RESULTS

A. Quantitative XPS study of bare BTO and BLT films

The integrated intensities of O $1s$, Bi $4f$, Ti $2p_{3/2}$, and/or La $3d$ core-level peaks, as well as their corresponding sensitivity factors with reference to the analyzer were used to determine the surface compositions of bare BTO and BLT films. The results shown in Table I indicate considerable bismuth and/or lanthanum excesses, and titanium deficiency with respect to the nominal compositions. According to the high-resolution electron microscopy (HREM) study of BTO and BLT powder compounds,[10,23] the surface nonstoichiometry of BTO originates from a very thin amorphous bismuth oxide layer enclosing the crystal edge, and that of BLT results from specific surface configurations that consist of an outermost Bi-rich region followed by a La-rich region before arriving at the stoichiometric bulk. The significant surface excess of lanthanum tends to occupy the cation site in fluorite-like $(Bi_2O_2)^{2+}$ layers, leading to the surface intergrowth defects of BLT as shown in Fig. 2(b).[10] Since the surface nonstoichiometries in the powder compounds and

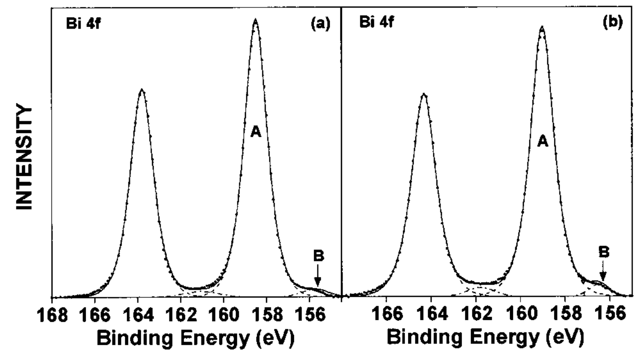

FIG. 3. Bi $4f$ core levels of bare (a) BTO and (b) BLT films. Dots correspond to experimental data; dashed lines to deconvoluted components; and solid lines to the sum of the deconvoluted components. Components: A, lattice Bi^{3+}; B, reduced bismuth species.

thin films are rather similar, the intergrowth defects of crystals characterized from the surface of powder compounds[10] are also expected to exist in thin films. However, some modifications of the thickness and form of the intergrowth defects in crystals of BLT films are probable, and a further HREM study is in progress in order to give a detailed insight into this feature.

Another characteristic of Table I is the noticeable oxygen deficiencies of BTO and BLT film surfaces, which can be related to the emergence of reduced bismuth species (see component B in Fig. 3; component A represents the lattice Bi^{3+}[28]) under ultra-high vacuum (UHV).[23] This correlation can be expressed as follows:

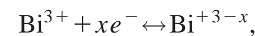

$$Bi^{3+} + xe^- \leftrightarrow Bi^{+3-x},$$

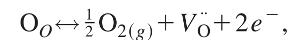

$$O_O \leftrightarrow \tfrac{1}{2}O_{2(g)} + V_O^{\cdot\cdot} + 2e^-,$$

where $0<x<3$. The bismuth reduction on exposure to UHV was also reported in XPS studies of $Bi_{4-x}La_xTi_3O_{12}$ powder compounds,[23] BTO single crystals,[29] SBT ceramics,[30] and SBT thin films.[31,32] These features indicate that the formation of $V_O^{\cdot\cdot}$ in Aurivillius phases should be related to the fragility of Bi-O bonds rather than the volatilization of bismuth,[18–21] as bismuth deficiency was never characterized in previous[23,31] or present XPS studies.

B. *Ex-situ* XPS studies of Pt-BTO and Pt-BLT interfaces

1. Ti 2p and/or La 3d core levels

Figure 4 shows Ti $2p$ core levels at the Pt-BTO and Pt-BLT interfaces, and Fig. 5 exhibits La $3d$ core levels at the Pt-BLT interfaces. Note that the Ti $2p$ and La $3d$ core-level states at the Pt-BLT interfaces cannot be observed when the Pt coverage takes place [see "virgin" 5, 10, and 20 Å in Figs. 4(b) and 5], whereas they become visible after heat treatments. In contrast, Ti $2p$ core levels at the Pt-BTO interfaces are not screened by thin Pt overlayers. These features may arise from the poor Pt thickness control, thus we will re-examine the overlayer thickness by the following equation:[33]

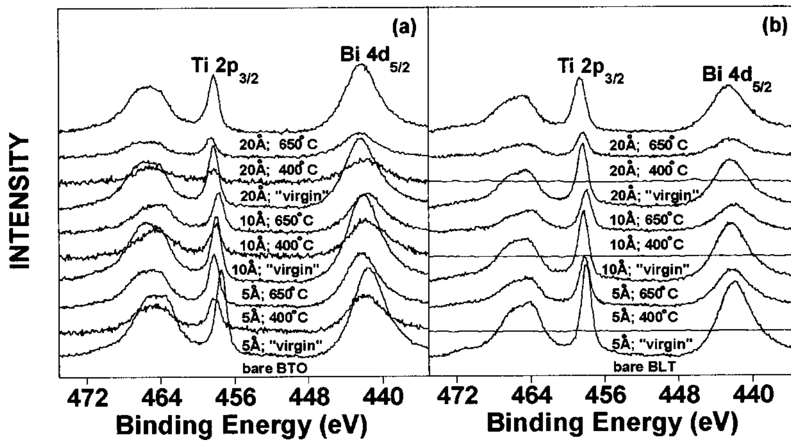

FIG. 4. Ti $2p$ and Bi $4d$ core levels at the (a) Pt-BTO and (b) Pt-BLT interfaces with different degrees of Pt coverage and heat treatments, as well as those of bare BTO and BLT films are also shown. The intensities of core-level states at the "virgin" Pt-BTO interfaces are multiplied by 2 due to their low intensities.

$$I_d = I_\infty [1 - \exp(-d/\lambda \sin\theta)],$$

where I_d is the integrated intensity of the thin overlayers, I_∞ is the integrated intensity of an infinitely thick pure substrate, d is the thickness of the thin overlayers, λ is the escape depth of outgoing photoelectrons, and θ is the photoelectron take-off angle relative to the sample surface. I_∞ is taken from the Pt $4f$ integrated intensity of a freshly sputtered Pt(111) film with a thickness of ~200 nm, λ of Pt $4f$ photoelectrons is close to 15 Å,[27] and θ is equal to 90°. The as-calculated Pt thicknesses of the various samples are given in Table II, and the results are self-consistent. They do not represent the exact thickness of the thin Pt overlayers, because (a) it is difficult to estimate the effects of surface contamination (carbon and adsorbed oxygen species) sandwiched between the Pt and complex oxide film surfaces, (b) further O_2 annealing could complicate the influences of (a), and (c) Pt $4f$ core levels at the interfaces include various Pt species (see Sec. III B 2) that could lead to an overestimation or underestimation of the Pt thickness. In spite of these potential difficulties, the calculated Pt thickness at the "virgin" Pt-BTO and Pt-BLT interfaces is in fair agreement with the nominal values estimated by the quartz balance installed in the sputtering apparatus. With O_2 annealing, the Pt thickness decreases, which corresponds to the interdiffusion of Pt into the film interior, i.e., the thermal drive-in.

These characteristics indicate that the absence of Ti $2p$ and La $3d$ core levels at the "virgin" Pt-BLT interfaces arises from the collective effects of Pt screening and specific surface configurations of the BLT crystals. The Pt coverage shadows Ti $2p$ and La $3d$ information in BLT films prior to O_2 annealing, but the thermal drive in of Pt on annealing leads to less significant screening effects. Consequently, the Ti $2p$ and La $3d$ core levels can again be observed. Due to the absence of intergrowth defects in BTO crystals,[10] the Ti $2p$ core-level states are always visible. From Table II we can also note that the Pt overlayers at the annealed Pt-BLT interfaces (400 and 650 °C) are always thicker than those at the annealed Pt-BTO, which implies that the specific surface configurations of BLT crystals behave as an *intrinsic* diffusion barrier to Pt.

2. Pt 4f core levels

Figures 6 and 7 show characteristically asymmetric Pt $4f$ core levels at the Pt-BTO and Pt-BLT interfaces, respectively. The Doniach-Šunjić function[34] coupled with a reasonable Gaussian contribution was used to deconvolute these core-level states that are elucidated as follows:

a. "Virgin" interfaces Both the regular line shapes in Figs. 6(a)–6(c) and 7(a)–7(c) and the peak positions (Pt $4f_{7/2}$) at 71.3–71.6±0.1 eV indicate that the as-deposited thin Pt overlayers are in a pure metallic state (indicated as component A).[27,28,35–38] However, another component, B, with lower binding energy (BE; Pt $4f_{7/2}$ at 67.1 and 67.6 ±0.1 eV for the Pt-BTO and Pt-BLT interfaces, respectively) emerges when the Pt coverage reaches ~20 Å [see Figs. 6(c) and 7(c)]. Note that no impurity state other than surface carbon and oxygen contamination was observed, and no Pt species with corresponding BE has been reported in the literature.[27,28,35–40] Further examining their chemical shifts with respect to component A, significant shifts of 4.3 and 3.6±0.1 eV towards the low BE side were determined for Pt-BTO and Pt-BLT interfaces, respectively, which suggests that component B originates from metallic compounds. Also

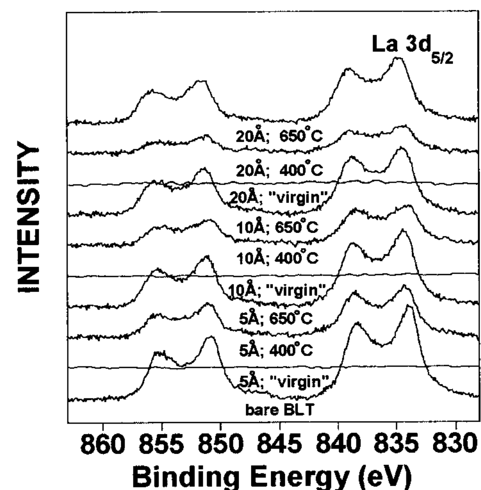

FIG. 5. La $3d$ core levels at the Pt-BLT interfaces with different degrees of Pt coverage and heat treatments. That of the bare BLT film is also shown.

TABLE II. The calculated thickness of thin Pt overlayers.

	Pt ~5 Å[a]		Pt ~10 Å[a]		Pt ~20 Å[a]	
Samples	Pt-BTO	Pt-BLT	Pt-BTO	Pt-BLT	Pt-BTO	Pt-BLT
"virgin"	6.0[b]	6.2	8.6	8.4	19.5	19.1
400 °C annealed	2.8	4.0	5.8	7.7	13.7	15.0
650 °C annealed	1.7	3.0	2.6	3.7	5.6	6.3

[a]The nominal thickness of thin Pt overlayers estimated by the quartz balance installed in the sputtering apparatus.

[b]The estimated thickness in Å, calculated from Ref. 33.

taking into account the reduced bismuth species emerging with increased Pt coverage (see component B in Fig. 8; component A represents contributions from lattice Bi^{3+}[28]), this metallic Pt species is related to the formation of a Bi-Pt alloy, however, its exact composition is unclear due to the lack of knowledge of Bi-Pt solubility.[41] Note also that component B is absent in Figs. 6(a), 6(b), 7(a), and 7(b), while considerable reduced bismuth species can be observed in Figs. 8(a), 8(b), 8(d), and 8(e). This feature may arise from that the empirical atomic sensitivity factor of Bi $4f$ photoelectrons is superior to that of Pt $4f$.[40]

The emergence of a Bi-Pt alloy was first suggested by Gutleben[31,32] in XPS studies of the Pt-SBT interface. However, we first report Pt $4f$ core-level evidence for a Bi-Pt alloy, and suggest that the strong Bi-Pt interaction in Aurivillius phases can lead to the formation of a Bi-Pt alloy.

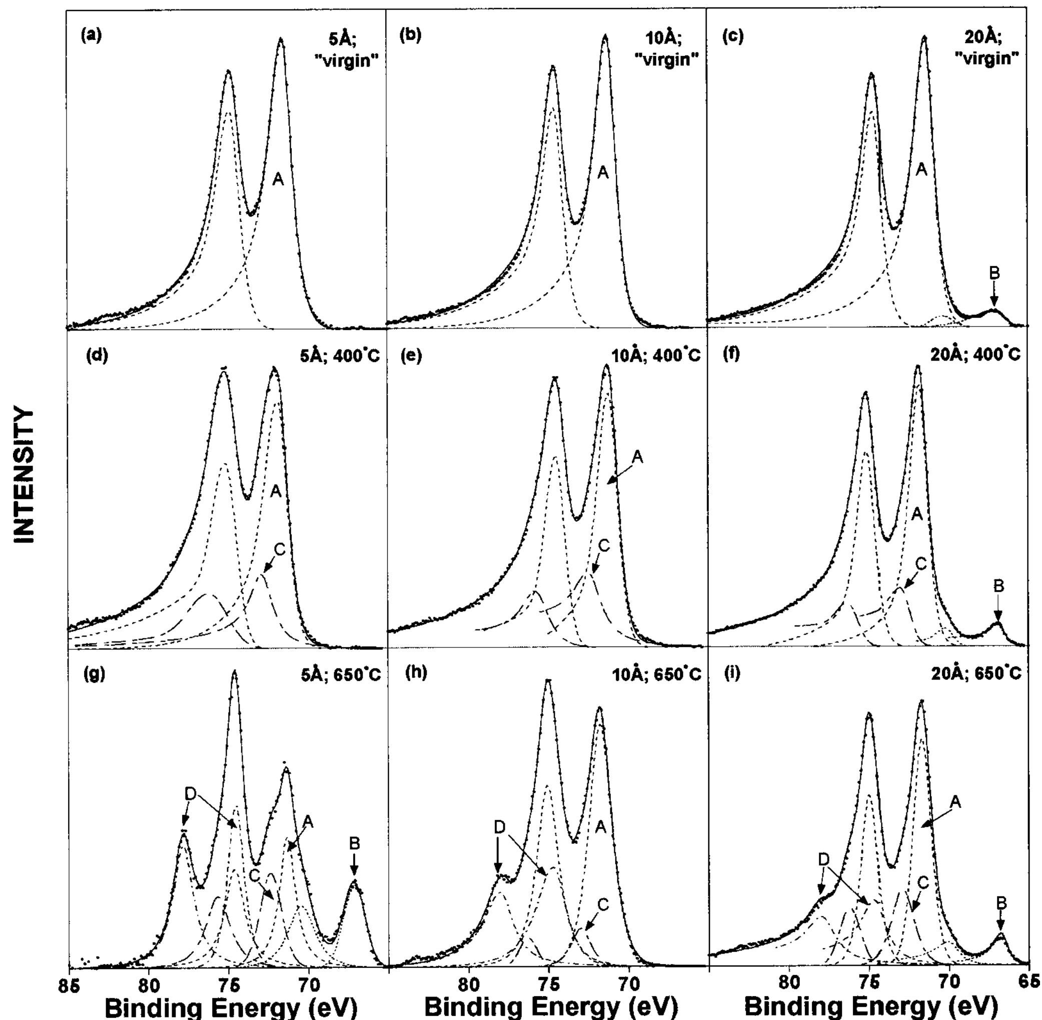

FIG. 6. (a)–(i) Pt $4f$ core levels at the Pt-BTO interfaces with different degrees of Pt coverage and heat treatments as indicated in each subset. Dots correspond to experimental data; dashed lines to deconvoluted components; and solid lines to the sum of the deconvoluted components. Components: A, pure metallic Pt; B, metallic Pt attributed to Bi-Pt alloy; C, Pt^{2+}; D, Pt^{4+}.

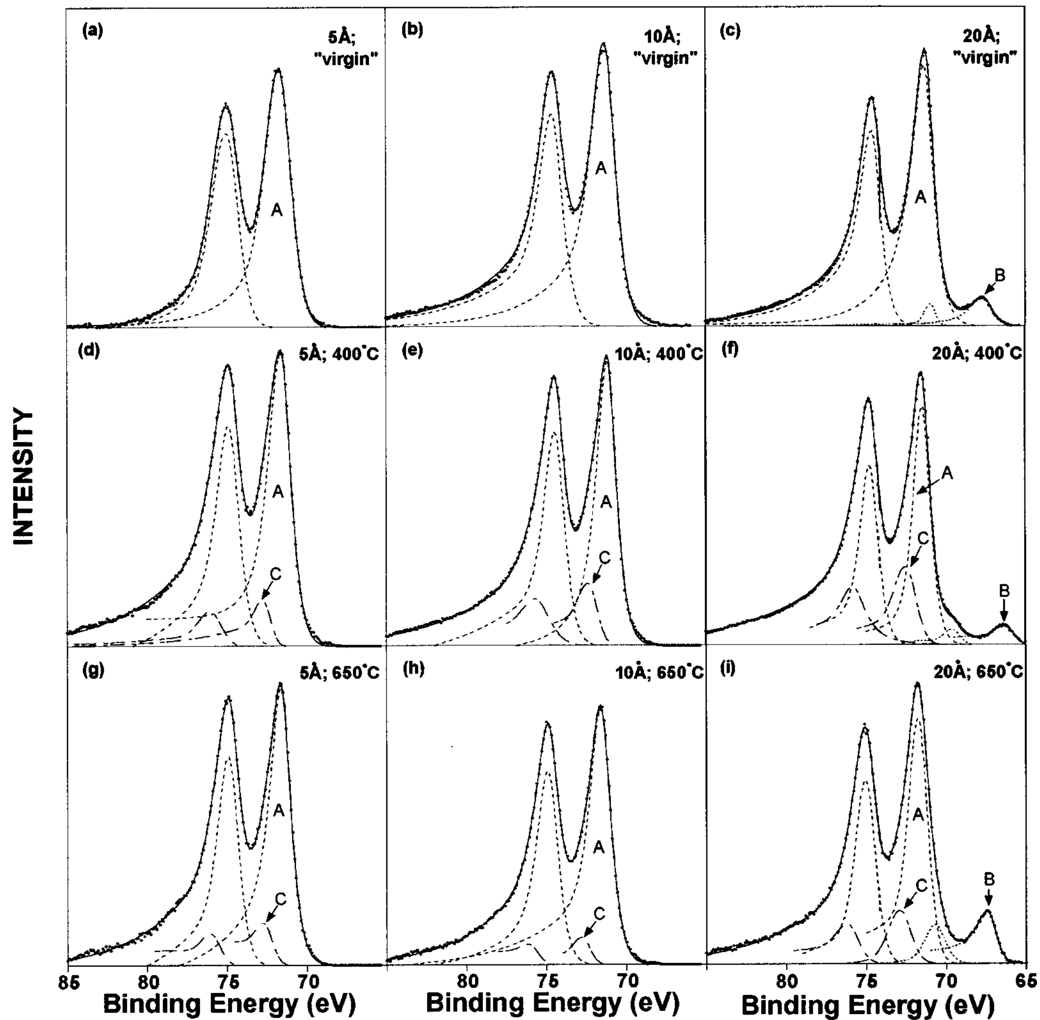

FIG. 7. (a)–(i) Pt 4f core levels at the Pt-BLT interfaces with different degrees of Pt coverage and heat treatments as indicated in each subset. Dots correspond to experimental data; dashed lines to deconvoluted components; and solid lines to the sum of the deconvoluted components. Components: A, pure metallic Pt, B, metallic Pt attributed to Bi-Pt alloy; C, Pt^{2+}.

b. 400 °C-annealed interfaces The intensity ratio of Pt $4f_{7/2}$ and Pt $4f_{5/2}$ in Fig. 6(d)–6(f) and 7(d)–7(f) deviates from the normal case for pure metallic Pt as shown in Figs. 6(a), 6(b), 7(a), and 7(b), which suggests that Pt species with higher oxidation state appear after O_2 annealing.[27,35,36] The curve deconvolution further indicates the emergence of component C possessing chemical shifts of $(1.1-1.3)\pm 0.1$ eV with respect to pure metallic Pt. Oxidized Pt species with similar chemical shifts, 1.5 (Ref. 27) and 1.3 eV (Ref. 36), have been assigned to PtO by Légaré *et al.* and Peuckert *et al.*, respectively. However, this does not mean that PtO is formed at the interfaces, since pure metallic Pt exhibits good oxidation resistance in flowing O_2 with atmospheric pressure.[36]

c. 650 °C-annealed interfaces Under these annealing conditions, the Pt 4f core levels at the Pt-BTO and Pt-BLT interfaces show very different line shapes [see Figs. 6(g)–6(i) and 7(g)–7(i)]. One more set of oxidized Pt species (component D) appears exclusively at the Pt-BTO interfaces with chemical shifts of $(3.0-3.2)\pm 0.1$ eV with respect to pure metallic Pt. Note that component D corresponds to Pt species with an oxidation state of +4, as the chemical shift of PtO_2 has been recorded from 2.4 to 3.4 eV depending on the compositions of studied samples.[35] Furthermore, Peuckert *et al.*[36] have indicated that the formation of Pt oxides is a very slow process that blocks the deep oxidation of bulk metallic Pt, and their growth rate is trivial at temperatures lower than ~900 K (at an O_2 pressure in 0.1 MPa in Ref. 36). In our case, this means that the formation of Pt oxides should eliminate Pt interdiffusion. The Pt thermal drive-in determined in Table II therefore definitively indicates that components C and D cannot be attributed to PtO and PtO_2, respectively. However, they do belong to the oxidation states of +2 and +4, respectively. It is thus reasonable to suggest that components C (Pt^{2+}) and D (Pt^{4+}) should arise from the substitution of Pt for lattice cations. More insights are given in Sec. IV.

In addition, the O_2 annealing qualitatively annihilates the Bi-Pt alloy at the interfaces, whereas the Pt thermal drive-in would allow it to form at relatively deeper interfaces. Due to

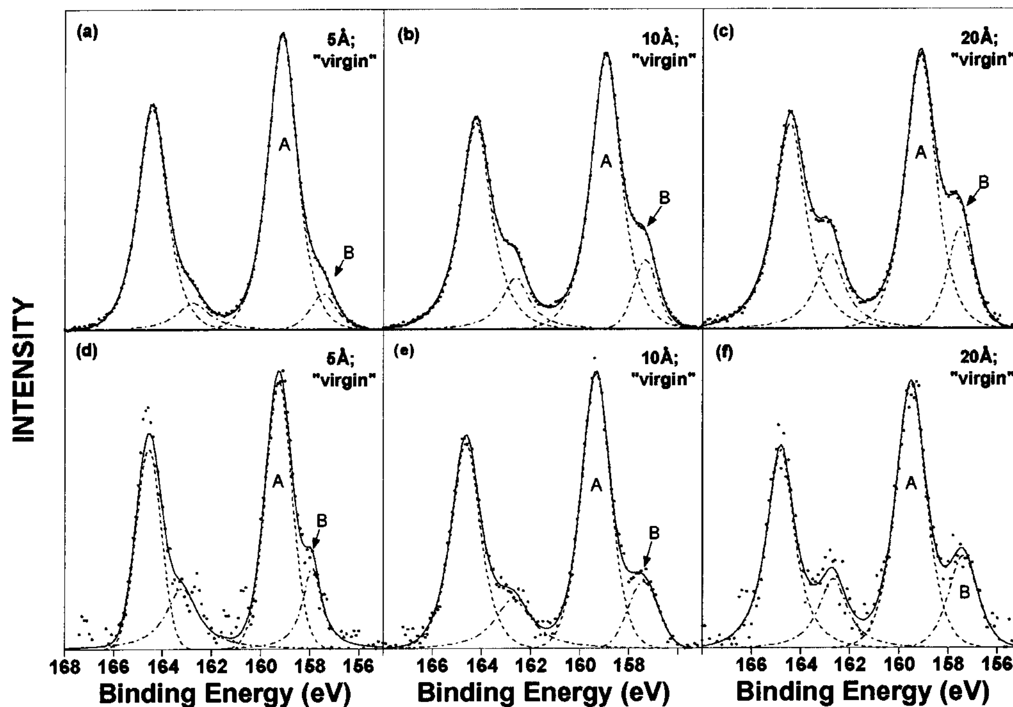

FIG. 8. Bi $4f$ core levels at the (a)–(c) Pt-BTO and (d)–(f) Pt-BLT interfaces with different degrees of Pt coverage as indicated in each subset. Dots correspond to experimental data; dashed lines to deconvoluted components; and solid lines to the sum of the deconvoluted components. Components: A, lattice Bi^{3+}; B, reduced bismuth species.

minimal Pt screening, ~1.7 Å (see Table II), at the Pt(5 Å)-BTO interface, the Bi-Pt alloy (component B) can be observed as shown in Fig. 6(g). The relatively thick Pt coverage at Pt(10 Å)-BTO, Pt(5 Å)-BLT, and Pt(10 Å)-BLT interfaces may make this component unobservable [see Figs. 6(h), 7(g), and 7(h), respectively]. For Pt(20 Å)-BTO and Pt(20 Å)-BLT interfaces [see Figs. 6(i) and 7(i)], the concentration of the Bi-Pt alloy should be very considerable, and the Pt screening is thus less important.

In summary, a Bi-Pt alloy always occurs in the vicinity of "virgin," 400 °C-, and 650 °C-annealed interfaces due to the strong Bi-Pt interaction. In terms of charge balance, this characteristic would enhance the formation of $V_{\mathrm{O}}^{\cdot\cdot}$. Furthermore, the Bi-Pt alloy could increase the leakage current of BTO and BLT capacitors with Pt as electrode(s).

IV. DISCUSSION

In *ex situ* XPS studies, Pt impurity defects (Pt^{2+} and Pt^{4+}) are indicated to arise from the substitution of Pt for lattice cations, and Pt^{4+} is present exclusively at the Pt-BTO interfaces in samples annealed at 650 °C. Detailed formation mechanisms of these impurities and their possible effects on ferroelectric degradation are elucidated as follows:

A. Pt impurity defects at the Pt-BTO interfaces

1. Isolated Pt impurity defects and spontaneous polarization degradation

Under O_2 annealing, the substitution of Pt for lattice cations occurs preferentially on sixfold symmetry sites,[42] and there are two sixfold sites, Ti(1) and Ti(2) (see Fig. 1), suitable for Pt substitution on the crystal surface of BTO. According to size arguments ($Pt^{2+}=0.80$ Å, $Pt^{4+}=0.625$ Å, and $Ti^{4+}=0.605$ Å),[42] Pt^{4+} should be the dominant impurity defects at 400 °C-annealed interfaces. However, it is Pt^{2+} that is observed [see Figs. 6(d)–6(f)], which suggests that the bonding characteristics of the perovskite-like slabs do govern the Pt/Ti substitution. From Postnikov *et al.*'s[29] electronic structure study of BTO, the strong hybridization between $3d$ and $2p$ states of Ti(2) and the apical O(4), respectively, plays an important role in its ferroelectricity. In contrast, Ti(1) does not show such strong hybridization with its coordinated oxygen ions.[29] In other words, Ti(1) is relatively more ionic, and Ti(2) is more covalent. Therefore, the substitution for Ti(2) qualitatively needs more driving force, e.g., higher annealing temperature, than for Ti(1); and the relatively ionic Pt^{2+} species will substitute preferentially for Ti(1), while the relatively covalent Pt^{4+} will replace Ti(2). This feature successfully interprets the exclusive presence of Pt^{4+} at the 650 °C-annealed Pt-BTO interfaces. Pt^{2+} and Pt^{4+} can be thus labeled as $\mathrm{Pt}_{\mathrm{Ti}(1)}''$ and $\mathrm{Pt}_{\mathrm{Ti}(2)}$, respectively. However, the closely filled $5d$ states of $\mathrm{Pt}_{\mathrm{Ti}(1)}''$ ($5d^8$) and $\mathrm{Pt}_{\mathrm{Ti}(2)}$ ($5d^6$) do not favor hybridization with O $2p$ states. $\mathrm{Pt}_{\mathrm{Ti}(1)}''$ and $\mathrm{Pt}_{\mathrm{Ti}(2)}$ thus tend to occupy the center of the octahedral clusters (schematized in Fig. 9). For simplicity, the structural model shown in Fig. 9 is in the idealized tetragonal symmetry ($I4/mmm$, No. 139) of Aurivillius phases, whereas the real symmetry of BTO is monoclinic including octahedral distortion and a-direction displacement of Bi^{3+} in the perovskitelike slabs.[8] In addition, one has to note that the polarizing effect of $\mathrm{Pt}_{\mathrm{Ti}(2)}$ is superior to that of $\mathrm{Pt}_{\mathrm{Ti}(1)}''$ result-

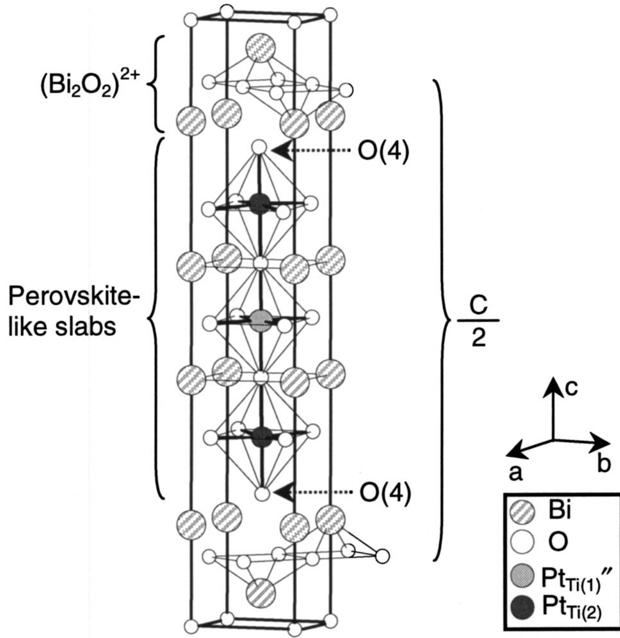

FIG. 9. The schematic geometry of $Pt_{Ti(1)}''$ (Pt^{2+}) and $Pt_{Ti(2)}$ (Pt^{4+}) in the perovskite-like slabs of $Bi_4Ti_3O_{12}$ (BTO; crystallographic data from Ref. 29 in $I4/mmm$).

ing in its relatively off-center shift with respect to $Pt_{Ti(1)}''$. The tendency of $Pt_{Ti(1)}''$ and $Pt_{Ti(2)}$ to occupy central positions would lead to a partial degradation of spontaneous polarization.[43] This ferroelectric degradation is primarily dominated by $Pt_{Ti(2)}$ defects, because the relatively ionic Ti(1) environment is not responsible for the ferroelectricity of BTO.[29] Since $Pt_{Ti(2)}$ only appears at the 650 °C-annealed Pt-BTO interfaces that are equivalent to the bottom-electrode interfaces of Pt/BTO/Pt capacitors, we suggest that top- and bottom-electrode interfaces should play different roles in the degradation of spontaneous polarization.

2. *Complex metal-impurity-oxygen-vacancy defect pairs and fatigue of BTO*

In titanate perovskites, $V_O^{\cdot\cdot}$ can combine with metal-impurity defects resulting in stable complex metal-impurity-oxygen-vacancy defect pairs.[15,43–45] Pöykkö *et al.*[15] further indicated that the defects pairs, $Pt_{Ti}''-V_O^{\cdot\cdot}$, in ferroelectric titanate perovskites are strongly polar and able to pin the polarizations of surrounding lattices inducing fatigue.

Taking these features into account, $V_O^{\cdot\cdot}$ (mobile point defects) induced by the formation of the Bi-Pt alloy can statistically meet immobile $Pt_{Ti(1)}''$ and $Pt_{Ti(2)}$ in the nearby interface region in the absence of the switching bias, leading to $Pt_{Ti(1)}''-V_O^{\cdot\cdot}$ and $Pt_{Ti(2)}-V_O^{\cdot\cdot}$ defect pairs.[15,43–45] Under the switching bias, $V_O^{\cdot\cdot}$ can move and redistribute throughout thin films.[43] Therefore, more $V_O^{\cdot\cdot}$ encounter $Pt_{Ti(1)}''$ and $Pt_{Ti(2)}$ resulting in more $Pt_{Ti(1)}''-V_O^{\cdot\cdot}$ and $Pt_{Ti(2)}-V_O^{\cdot\cdot}$ defect pairs, i.e., complex defect pairs becoming the dominant defects after bipolar reversals. Note that the primary driving force for the formation of these pairs is the atomic relaxation and rebonding in $(Pt_{Ti(1)}''O_5V_O^{\cdot\cdot})^{8-}$ and $(Pt_{Ti(2)}O_5V_O^{\cdot\cdot})^{6-}$ clusters.[15] Consequently, the movement of $Pt_{Ti(1)}''$ and $Pt_{Ti(2)}$ towards their nearest-neighbor $V_O^{\cdot\cdot}$ induces the formation of complex defect pairs. This procedure qualitatively does not consume energy, since $V_O^{\cdot\cdot}$ is a vacant site.[15] However, the doubly charged $Pt_{Ti(2)}-V_O^{\cdot\cdot}$ pairs are relatively unstable in lattices, so they would capture two electrons during bipolar reversals in order to maintain the charge balance of the native $(Pt_{Ti(2)}O_6)^{8-}$ clusters, leading to $Pt_{Ti(2)}''-V_O^{\cdot\cdot}$ pairs. This behavior qualitatively makes the degree of atomic relaxation and rebonding more significant, thus leading to more polar $Pt_{Ti(2)}''-V_O^{\cdot\cdot}$ pairs. These polar $Pt_{Ti(1)}''-V_O^{\cdot\cdot}$ and $Pt_{Ti(2)}''-V_O^{\cdot\cdot}$ pairs are schematized in Figs. 10(a)–10(c) and their respective polarizations are indicated as P_1 and P_2. In ferroelectrics, such polar defect pairs are strongly bound once being formed, and therefore, they are nonswitchable under bipolar reversals.[15,46,47] This feature makes the environment surrounding the defect pairs more rigid. Therefore, the degree of *a*-direction displacement of Bi^{3+} is reduced, while this cation displacement is crucial for the polarization of BTO.[8] Consequently, these polar defect pairs could pin the polarizations of surrounding lattices, qualitatively leading to the fatigue of BTO. Note that the more polar $Pt_{Ti(2)}''-V_O^{\cdot\cdot}$ pairs should have more significant effects on fatigue compared to $Pt_{Ti(1)}''-V_O^{\cdot\cdot}$. In addition, the $Pt_{Ti(1)}''-V_O^{\cdot\cdot}-Pt_{Ti(2)}$ defects [schematized in Fig. 10(d)] should have less influences on fatigue, because the reverse polarizations of the $Pt_{Ti(1)}''-V_O^{\cdot\cdot}$ and $Pt_{Ti(2)}-V_O^{\cdot\cdot}$ centers make their global polarity relatively insignificant.

The characteristics elucidated above are closely relevant to "the interface scenario" of Pt/PZT/Pt capacitors,[6,12–14] and strongly refer to that BTO capacitors with Pt as electrode(s) can be immune to fatigue by inserting a diffusion barrier between BTO and the Pt electrode or by replacing the Pt electrode with a conductive oxide. This idea is supported by Watanabe *et al.*'s study[48] that Pt/BTO//$CaRuO_3$ and Pt/BTO//$SuRuO_3$ capacitors annealed at 800 and 880 °C, respectively, in flowing O_2 (without post-annealing after the deposition of the Pt top electrodes) exhibited good fatigue endurance up to 7.8×10^{10} switching cycles. Although interfacial phases and/or defects might exist in BTO//$CaRuO_3$ and BTO//$SrRuO_3$ interfaces, their effects on fatigue should be insignificant. This fair agreement suggests that the fatigue properties of BTO can be attributed to "the interface scenario,"[6,12–14] and that top- and bottom-electrode interfaces should play different roles in fatigue. In addition, this interface scenario indicates that fatigue resistance of ferroelectric capacitors with conductive oxides as electrode(s) arises from the absence of metal-impurity defects at the interfaces rather than the conductive oxides behaving as the $V_O^{\cdot\cdot}$ sink.[15]

B. Pt impurity defects at the Pt-BLT interfaces

Due to the surface intergrowth defects of BLT crystals [see Fig. 2(b)], Pt would substitute for cations in BiO_2, TiO_2, and (Bi,La)O planes, and/or insert into cation vacancies, V_{Bi}''' and/or V_{La}''', in the (Bi,La)O and BiO_2 planes upon annealing in O_2. These sites should be relatively ionic, thus leading to the exclusive presence of Pt^{2+} [see Figs.

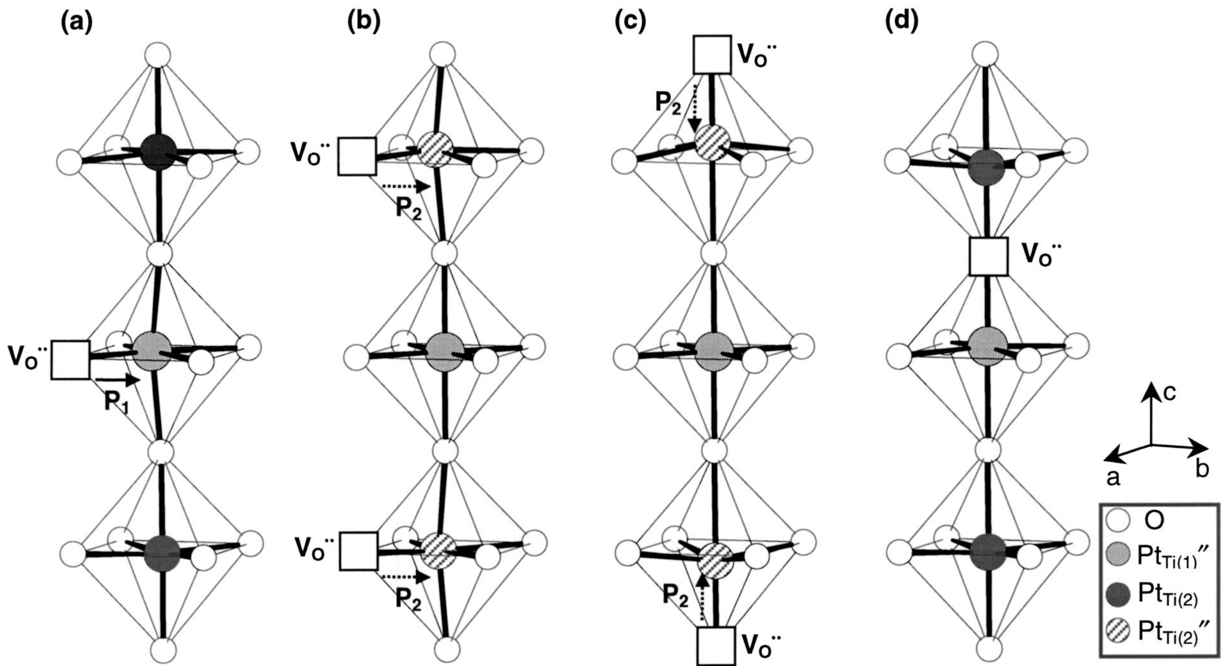

FIG. 10. The schematic geometry of (a) $Pt_{Ti(1)}''-V_O^{\cdot\cdot}$, (b) and (c) $Pt_{Ti(2)}''-V_O^{\cdot\cdot}$, and (d) $Pt_{Ti(1)}''-V_O^{\cdot\cdot}-Pt_{Ti(2)}$ defects in the perovskite-like slabs of $Bi_4Ti_3O_{12}$ (BTO); P_1 and P_2 represent local polarizations of $Pt_{Ti(1)}''-V_O^{\cdot\cdot}$ and $Pt_{Ti(2)}''-V_O^{\cdot\cdot}$ pairs, respectively. Crystallographic data from Ref. 29 in $I4/mmm$.

7(d)–7(i)]. In addition, $Pt_{Ti(1)}''$ and $Pt_{Ti(2)}$ might occur at the deeper interfaces (>5 nm, beyond the depth limit of XPS analyses), where the regular Aurivillius structure exists.[10] Further taking into account the thicker Pt overlayers at annealed Pt-BLT interfaces (400 and 650 °C) compared to those at annealed Pt-BTO (see Table II), we suggest that the bonding environments around the surface intergrowth defects should be less preferable for Pt.

Since the Pt impurities of BLT predominantly localize in the surface region exhibiting intergrowth defects rather than the regular Aurivillius structure, their effects on the ferroelectric degradation should be qualitatively limited. As a consequence, BLT shows good fatigue endurance. In addition, the surface intergrowth defects of BLT should intrinsically degrade its spontaneous polarization.

Nevertheless, Wu *et al.*[21] reported that Pt/BLT/Pt capacitors annealed at 650 °C in flowing O_2 and then post-annealed at 650 °C after the deposition of the Pt top electrodes are not immune to fatigue, and the switchable polarization reduces upon decreasing the cycling field and cycling frequency. Since the bottom-electrode interfaces were subjected twice to heat treatments at 650 °C,[21] metallic Pt from the bottom electrode and Pt^{2+} from the bottom-electrode interfaces can diffuse further into the BLT film interior. Therefore, $Pt_{Ti(1)}''$, $Pt_{Ti(2)}$, $Pt_{Ti(1)}''-V_O^{\cdot\cdot}$, and $Pt_{Ti(2)}-V_O^{\cdot\cdot}$ defects may occur at the relatively deeper bottom-electrode interfaces. Due to the similarity in crystal and electronic structures of BTO and BLT,[49] "the interface scenario" of BTO should also hold for BLT. Therefore, mobile $V_O^{\cdot\cdot}$ would have more time to combine with Pt impurities by decreasing the cycling field and cycling frequency, leading to more $Pt_{Ti(1)}''-V_O^{\cdot\cdot}$ and $Pt_{Ti(2)}-V_O^{\cdot\cdot}$ pairs at the relatively deeper bottom-electrode interfaces of Pt/BLT/Pt (Ref. 21) capacitors. Meanwhile, electronic charge carriers move slower, which gives $Pt_{Ti(2)}-V_O^{\cdot\cdot}$ more time to trap electrons, leading to more $Pt_{Ti(2)}''-V_O^{\cdot\cdot}$ pairs. Consequently, $Pt_{Ti(1)}''-V_O^{\cdot\cdot}$ and $Pt_{Ti(2)}''-V_O^{\cdot\cdot}$ pairs at the bottom-electrode interfaces would induce the cycling field- and frequency-dependent fatigue properties of Pt/BLT/Pt capacitors (Ref. 21). It is worth noticing that Pt/SBT/Pt capacitors post-annealed at 900 and 950 °C after the deposition of the Pt top electrodes were reported to exhibit fatigue degradation, while those post-heat-treated at 800 °C are immune to fatigue.[50] This phenomenon is similar to the fatigue failure of Pt/BLT/Pt capacitors post-annealed at 650 °C (Ref. 21), and may also arise from the formation of defect pairs at the relatively deeper Pt-ferroelectrics interfaces. Note also that the bare surface of crystals in SBT thin films was indicated to consist of surface defects.[22]

In summary, fatigue in BTO and BLT capacitors with Pt as electrode(s) should result from that the polar metal-impurity-oxygen-vacancy defect pairs pin the polarizations of surrounding lattices. Pöykkö *et al.*[15] first proposed this mechanism for fatigue in simple titanate perovskites, whereas the current *ex situ* XPS study suggests that this mechanism should also hold in Aurivillius BTO and BLT (layered titanate perovskites). An extensive HREM study of Pt-BTO and Pt-BLT interfaces is under way in order to confirm the defect-pairs model proposed by the *ex situ* XPS study.

V. CONCLUSION

Pt-$Bi_4Ti_3O_{12}$(BTO) and Pt-$Bi_{3.25}La_{0.75}Ti_3O_{12}$(BLT) interfaces in Pt/ferroelectrics/Pt capacitors were simulated and

studied by *ex situ* XPS analyses. Three important results are summarized.

(1) The bare surface of crystals in BLT thin films consists of intergrowth defects.

(2) The strong Bi-Pt interaction always induces Bi-Pt alloy at the interfaces, leading to the accumulation of oxygen vacancies ($V_O^{\cdot\cdot}$).

(3) At the 400 °C- and 650 °C-annealed Pt-BTO and Pt-BLT interfaces, the Pt substitution at the BTO and BLT lattices results in Pt impurity defects, which can combine with $V_O^{\cdot\cdot}$ resulting in complex metal-impurity-oxygen-vacancy defect pairs. The complex defect pairs at the Pt-BTO interfaces are polar, nonswitchable, and able to pin polarizations of surrounding lattices inducing fatigue. The intergrowth defects of BLT crystals behave as an intrinsic diffusion barrier to Pt, and therefore, the harmful defect pairs occurring at the Pt-BTO interfaces are practically absent for the Pt-BLT interfaces, which could be associated with the reported different fatigue properties of BTO and BLT capacitors.

ACKNOWLEDGMENTS

The authors thank Dr. Yves Piffard and Dr. Laurie Hill for helpful discussions, and Dr. Pierre-Yves Tessier for thin Pt overlayers deposition.

*Present address: Max-Planck-Institut für Mikrostrukturphysik, Weinberg 2, D-06120, Halle (Saale), Germany. Electronic mail: cmingwen@mpi-halle.mpg.de

†Author to whom correspondence should be addressed. Electronic mail: caldes@cnrs-imn.fr FAX: 33-2-39-95. Present address: 2, rue de la Houssinière, B. P. 32229, 44322 Nantes Cedex 3, France.

[1] C. A-Paz de Araujo, J. D. Cuchiaro, L. D. McMillan, M. C. Scott, and J. F. Scott, Nature (London) **374**, 627 (1995).

[2] B. H. Park, B. S. Kang, S. D. Bu, T. W. Noh, J. Lee, and W. Jo, Nature (London) **401**, 682 (1999).

[3] H. N. Al-Shareef, O. Auciello, and A. I. Kingon, J. Appl. Phys. **77**, 2146 (1995).

[4] R. Dat, D. J. Lichtenwalner, O. Auciello, A. I. Kingon, Appl. Phys. Lett. **64**, 2673 (1994).

[5] R. Ramesh, B. Dutta, T. S. Ravi, J. Lee, T. Sands, and V. G. Keramidas, Appl. Phys. Lett. **64**, 1588 (1994).

[6] A. K. Tagantsev, I. Stolichnov, E. L. Colla, and N. Setter, J. Appl. Phys. **90**, 1387 (2001).

[7] H. N. Lee, D. Hesse, N. Zakharov, and U. Gösele, Science **296**, 2006 (2002).

[8] A. D. Rae, J. G. Thompson, R. L. Withers, and A. C. Willis, Acta Crystallogr., Sect. B: Struct. Sci. **46**, 474 (1990).

[9] M.-W. Chu, M. T. Caldes, Y. Piffard, A.-M. Marie, E. Gautier, O. Joubert, M. Ganne, and L. Brohan, J. Solid State Chem. **172**, 389 (2003).

[10] M.-W. Chu, M. T. Caldes, L. Brohan, M. Ganne, O. Joubert, and Y. Piffard, Chem. Mater. (to be published).

[11] A. I. Kingon, Nature (London) **401**, 658 (1999).

[12] J. J. Lee, C. L. Thio, and S. B. Desu, J. Appl. Phys. **78**, 5073 (1995).

[13] E. L. Colla, D. V. Taylor, A. K. Tagantsev, and N. Setter, Appl. Phys. Lett. **72**, 2478 (1998).

[14] Q. Jiang, W. Cao, and L. E. Cross, J. Am. Ceram. Soc. **77**, 211 (1994).

[15] S. Pöykkö and D. J. Chadi, Phys. Rev. Lett. **83**, 1231 (1999).

[16] J. Nuffer, D. C. Lupascu, J. Rödel, and M. Schroeder, Appl. Phys. Lett. **79**, 3675 (2001).

[17] B. H. Park, S. J. Hyun, S. D. Bu, T. W. Noh, J. Lee, H.-D. Kim, T. H. Kim, and W. Jo, Appl. Phys. Lett. **74**, 1907 (1999).

[18] D. Dimos, H. N. Al-Shareef, W. L. Warren, and B. A. Tuttle, J. Appl. Phys. **80**, 1682 (1996).

[19] H. N. Al-Shareef, D. Dimos, T. J. Boyle, W. L. Warren, and B. A. Tuttle, Appl. Phys. Lett. **68**, 690 (1996).

[20] D. Wu, A. Li, H. Ling, T. Yu, Z. Liu, and N. Ming, Appl. Phys. Lett. **76**, 2208 (2000).

[21] D. Wu, A. Li, T. Zhu, Z. Liu, and N. Ming, J. Appl. Phys. **88**, 5941 (2000).

[22] O. Auciello, A. R. Krauss, J. Im, D. M. Gruen, E. A. Irene, R. P. H. Chang, and G. E. McGuire, Appl. Phys. Lett. **69**, 2671 (1996).

[23] M.-W. Chu, M. Ganne, M. T. Caldes, and L. Brohan, J. Appl. Phys. **91**, 3178 (2002).

[24] P. C. Joshi and S. B. Krupanidhi, J. Appl. Phys. **72**, 5827 (1992).

[25] P. C. Joshi and S. B. Desu, J. Appl. Phys. **80**, 2349 (1996).

[26] M.-W. Chu, M. Ganne, P.-Y. Tessier, D. Eon, M. T. Caldes, and L. Brohan, Mater. Sci. Semicond. Process. **5**, 179 (2003).

[27] P. Légaré, G. Lindauer, L. Hilaire, G. Maire, J.-J. Ehrhardt, J. Jupille, A. Cassuto, C. Guillot, and J. Lecante, Surf. Sci. **198**, 69 (1988).

[28] C. D. Wagner, W. M. Riggs, L. E. Davis, J. F. Moulder, and G. E. Muilenberg, *Handbook of XPS* (Perkin-Elmer, Minneapolis, MN, 1979).

[29] A. V. Postnikov, St. Bartkowski, F. Mersch, M. Neumann, E. Z. Kurmaev, V. M. Cherkashenko, S. N. Nemnonov, and V. R. Galakhov, Phys. Rev. B **52**, 11 805 (1995).

[30] A. C. Palanduz and D. M. Smyth, J. Electroceram. **5**, 21 (2000).

[31] C. D. Gutleben, in *Ferroelectric Thin Film V*, edited by S. B. Desu, R. Ramesh, B. A. Tuttle, R. E. Jones, and I. K. Yoo, MRS Symposia Proceedings No. 433 (Materials Research Society, Pittsburgh, 1996), p. 109.

[32] C. D. Gutleben, Appl. Phys. Lett. **71**, 3444 (1997).

[33] A. J. Hartmann and R. N. Lamb, Curr. Opin. Solid State Mater. Sci. **2**, 511 (1997).

[34] S. Doniach and M. Šunjić, J. Phys. C **3**, 285 (1970).

[35] J. Sedláček, L. Hilaire, P. Légaré, and G. Maire, Surf. Sci. **115**, 541 (1982).

[36] M. Peuckert and H. P. Bonzel, Surf. Sci. **145**, 239 (1984).

[37] A. Dauscher, L. Hilaire, J. C. Spirlet, W. Müller, and G. Maire, Surf. Sci. **204**, 161 (1988).

[38] S. Hüfner and G. K. Wertheim, Phys. Rev. B **11**, 678 (1975).

[39] S. Hüfner, *Photoelectron Spectroscopy: Principles and Applications*, 2nd ed. (Springer-Verlag, Berlin, 1995), p. 459.

[40] D. Briggs and M. P. Seah, *Practical Surface Analysis*, 1st ed. (Wiley, Chichester, 1983), pp. 511–520.

[41] T. B. Massalski, H. Okamoto, P. R. Subramanian, and L. Kacprzak, *Binary Alloy Phase Diagrams*, 2nd ed. (ASM International, Ohio, 1992), Vol. 1, p. 777.

[42] R. D. Shannon, Acta Crystallogr., Sect. A: Cryst. Phys., Diffr., Theor. Gen. Crystallogr. **32**, 751 (1976).
[43] E. Siegel and K. A. Müller, Phys. Rev. B **20**, 3587 (1979).
[44] E. Siegel and K. A. Müller, Phys. Rev. B **19**, 109 (1979).
[45] O. F. Schirmer, W. Berlinger, and K. A. Müller, Solid State Commun. **16**, 1289 (1975).
[46] W. L. Warren, B. A. Tuttle, and D. Dimos, Appl. Phys. Lett. **67**, 1426 (1995).
[47] W. L. Warren, D. Dimos, G. E. Pike, K. Vanheusden, and R. Ramesh, Appl. Phys. Lett. **67**, 1689 (1995).
[48] T. Watanabe, H. Funakubo, and K. Saito, J. Mater. Res. **16**, 303 (2001).
[49] Y. Shimakawa, Y. Kubo, Y. Tauchi, H. Asano, T. Kamiyama, F. Izumi, and Z. Hiroi, Appl. Phys. Lett. **79**, 2791 (2001).
[50] J. S. Zhao, J. E. Lim, M. J. Cho, C. S. Hwang, and S.-H. Kim, Appl. Phys. Lett. **81**, 1477 (2002).